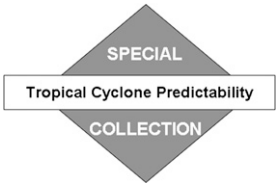

Validation and Interpretation of Adjoint-Derived Sensitivity Steering Vector as Targeted Observation Guidance

SHIN-GAN CHEN AND CHUN-CHIEH WU

Department of Atmospheric Sciences, National Taiwan University, Taipei, Taiwan

JAN-HUEY CHEN

NOAA/Geophysical Fluid Dynamics Laboratory, Princeton, New Jersey

KUN-HSUAN CHOU

Department of Atmospheric Sciences, Chinese Culture University, Taipei, Taiwan

(Manuscript received 4 May 2010, in final form 1 February 2011)

ABSTRACT

The adjoint-derived sensitivity steering vector (ADSSV) has been proposed and applied as a guidance for targeted observation in the field programs for improving tropical cyclone predictability, such as The Observing System Research and Predictability Experiment (THORPEX) Pacific Asian Regional Campaign (T-PARC). The ADSSV identifies sensitive areas at the observing time to the steering flow at the verifying time through adjoint calculation. In addition, the ability of the ADSSV to represent signals of influence from synoptic systems such as the midlatitude trough and the subtropical high prior to the recurvature of Typhoon Shanshan (2006) has also been demonstrated.

In this study, the impact of initial perturbations associated with the high or low ADSSV sensitivity on model simulations is investigated by systematically perturbing initial vorticity fields in the case of Shanshan. Results show that experiments with the perturbed initial conditions located in the high ADSSV area (i.e., the midlatitude trough and the subtropical high) lead to more track deflection relative to the unperturbed control run than experiments with perturbations in the low sensitivity area. The evolutions of the deep-layer-mean steering flow and the direction of the ADSSV are compared to provide conceptual interpretation and validation on the physical meaning of the ADSSV. Concerning the results associated with the perturbed regions in high sensitivity regions, the variation of the steering flow within the verifying area due to the initial perturbations is generally consistent with that of the direction of the ADSSV. In addition, the bifurcation between the ADSSV and the steering change becomes larger with the increased integration time. However, the result for the perturbed region in the low-sensitivity region indicates that the steering change does not have good agreement with the ADSSV. The large initial perturbations to the low-sensitivity region may interact with the trough to the north due to the nonlinearity, which may not be accounted for in the ADSSV. Furthermore, the effect of perturbations specifically within the sensitive vertical layers is investigated to validate the vertical structure of the ADSSV. The structure of kinetic energy shows that the perturbation associated with the trough (subtropical high) specifically in the mid-to-upper (mid-to-lower) troposphere evolves similarly to that in the deep-layer troposphere, leading to comparable track changes. A sensitivity test in which perturbations are locally introduced in a higher-sensitivity area is conducted to examine the different impact as compared to that perturbed with the broader synoptic feature.

1. Introduction

Additional observations made in most sensitive regions are expected to reduce uncertainties in the initial condition and thus decrease errors in numerical forecasts. This concept is referred to as the targeted (adaptive) observation, which has been one of the most active research and forecasting issues for improving tropical cyclone (TC) predictions (Langland 2005; Wu 2006). In practice, many targeted observation methods have been commonly applied to design optimal flight routes in operational aircraft surveillance missions conducted by the National Oceanic and Atmospheric Administration

Corresponding author address: Chun-Chieh Wu, Dept. of Atmospheric Sciences, National Taiwan University, No. 1, Sec. 4, Roosevelt Rd., Taipei 106, Taiwan.
E-mail: cwu@typhoon.as.ntu.edu.tw

DOI: 10.1175/2011MWR3490.1

(NOAA) in the Atlantic basin since 1997 (Aberson and Franklin 1999; Aberson 2002, 2003) and by the Dropwindsonde Observations for Typhoon Surveillance near the Taiwan Region (DOTSTAR) project (Wu et al. 2005) for western North Pacific typhoons since 2003. In the summer of 2008, the issue of targeted observation has also been extensively explored in the field campaign, The Observing System Research and Predictability Experiment (THORPEX) Pacific Asian Regional Campaign (T-PARC; Elsberry and Harr 2008). In addition, the value and impact of targeted observations on improving TC track forecasts or reducing forecast errors have been evaluated and addressed in many studies (e.g., Aberson 2003; Wu et al. 2007b; Yamaguchi et al. 2009; Harnisch and Weissmann 2010; Weissmann et al. 2011), while assimilating observational data into the numerical models is likely to lead to forecast degradation in some cases (Aberson 2008).

Targeted observation techniques that have been developed recently roughly fall into two types. One is based on ensemble forecasts, including ensemble deep-layer-mean (DLM) wind variance (Aberson 2003), ensemble transform Kalman filter (ETKF; Bishop et al. 2001; Majumdar et al. 2002), and ensemble sensitivity using the linear–regression relationship (Ancell and Hakim 2007). The other is based on the adjoint technique, including singular vectors (SVs; Buizza and Montani 1999; Peng and Reynolds 2006; Chen et al. 2009; Kim and Jung 2009a,b; Yamaguchi et al. 2009), and the adjoint-derived sensitivity steering vector (ADSSV; Wu et al. 2007a, 2009a). Several distinct targeted observation guidance products have been compared by using TCs in the Atlantic Ocean (Majumdar et al. 2006; Reynolds et al. 2007) and in the western North Pacific (Wu et al. 2009b) to not only highlight the unique dynamical features affecting TC motion, but also provide reliable information for facilitating targeted observations.

By appropriately defining the response functions to represent the typhoon steering flow at the verifying time (see section 2a), the ADSSV is calculated by the adjoint modeling system (Errico 1997; Zou et al. 1997) of the fifth-generation Pennsylvania State University–National Center for Atmospheric Research (PSU–NCAR) Mesoscale Model (MM5). It identifies sensitive areas at the observing time that would affect the typhoon steering flow at the verifying time. The ADSSV method would not only be applied as one of the targeted guidance products for typhoon surveillance missions, but would also provide dynamical interpretation of the distinct weather systems affecting TC motion. In addition to showing the validity of ADSSV for Typhoons Meari and Mindulle (2004), Wu et al. (2007a) identified signals of the binary interaction between Typhoons Fengshen and Fungwong (2002) using the ADSSV method. Furthermore, Wu et al. (2009a) demonstrated that the ADSSV captures signals indicating the influences of the large-scale midlatitude trough and the subtropical high prior to the recurvature of Typhoon Shanshan (2006), and such influences are verified by conducting potential vorticity (PV) analysis.

Hoover (2009) and Hoover and Morgan (2010) suggested that the displacement of a TC at the final time can have some nonnegligible influence on zonal and meridional steerings, which are possibly not related to the instantaneous steering effect. To address this issue, clarifications have been made in Wu et al. (2009c). It was shown that no perturbation is introduced for the ADSSV calculation in either the forward or the backward integrations. In other words, the TC at the final time is exactly located at the center of the verifying area. Preliminary results based on perturbing the initial condition associated with the midlatitude trough were shown to provide interpretation of the ADSSV sensitivity in Wu et al. (2009c). The effect of the perturbed field on the change in the steering flow was demonstrated. In this paper, physical interpretation and validity of the ADSSV are explored in detail based on the same case study of Typhoon Shanshan (2006).

In addition, the fixed verifying area may also be an issue of concern. At least three fixed verifying regions have been used to calculate the adaptive observation guidance for the T-PARC field experiment. However, those were only applied to targeted observation guidance such as the SVs or ETKF. For the ADSSV, the verifying area centered at the final-time TC is still used to calculate its sensitivity. The $20° \times 20°$ (for SVs and ETKF) and 600 km $\times$ 600 km (for ADSSV) verifying regions centered at the final-time TC had been used to conduct comparison studies such as Wu et al. (2009b). Thus, for the calculation of the ADSSV, the TC at the final time is always at the center of the verifying area.

Validating and investigating the applicability of the sensitive areas predicted by targeted observation techniques is an interesting topic in the field of targeted observation and data assimilation. The properties and characteristics of sensitive area prediction had been extensively examined and addressed both from the perspective of SVs by Buizza and Montani (1999), Peng and Reynolds (2006), as well as Chen et al. (2009) and through the ETKF method by Petersen et al. (2007) and Majumdar et al. (2011). Although the validity of the linear operator assumption in the adjoint model used to calculate the ADSSV has been examined in Wu et al. (2007a, 2009a), the ADSSV sensitivity signal remains to be validated and interpreted by perturbing the initial flow fields. Following the results from Wu et al. (2009a,c), the goal of this paper is to examine how perturbations in

regions with high or low ADSSV sensitivity in the initial condition would impact track simulation and the steering flow of Shanshan. The methodology of the ADSSV and procedure of systematically perturbing the initial field are briefly introduced in section 2. The results of the track simulation and the impacts on the mean background steering flow in different experiments as well as their interpretations are presented in section 3 whereas section 4 summarizes the study.

2. Methodology and experimental design

a. ADSSV

Since detailed ADSSV methodology has been described in Wu et al. (2007a, 2009a), provided here is a brief description of some details following these two papers. The verifying area in which the response functions are defined is an area (square of 600 km $\times$ 600 km typically) centered at the TC location at the verifying time simulated by the MM5 nonlinear model (i.e., the forward model). Note that this TC location is derived from the exact forward model simulation with no ambiguity. The two response functions are R_1, the deep-layer area-average wind (Wu et al. 2003) of the zonal component u between 0.875 and 0.225 sigma levels (roughly between 850 and 250 hPa) and R_2, the deep-layer average of the meridional component v of the wind vector. After the axisymmetric components of the strong cyclonic flow around the TC center are averaged out, the vector of (R_1, R_2) represents the mean background steering flow across the TC center at the verifying time. This idea basically follows the well-known steering concept (Chan and Gray 1982; Wu and Emanuel 1993).

As indicated in Wu et al. (2007a), $\partial R/\partial\varsigma$ (ς stands for the vorticity field) is adopted as an essential metric to represent the ADSSV with clear physical meanings. Thus, the ADSSV associated with the vorticity field is

$$\mathrm{ADSSV} \equiv \left(\frac{\partial R_1}{\partial \varsigma}, \frac{\partial R_2}{\partial \varsigma}\right), \tag{1}$$

where the magnitude of ADSSV represents the degree of sensitivity. Meanwhile, the direction of the ADSSV indicates the direction toward which the steering flow would move at the verifying time with respect to a vorticity perturbation placed at that point at the observing time. In other words, the ADSSV calculated from the MM5 adjoint modeling system shows the sensitivity of the average background steering flow at the verifying time to the flow (vorticity) fields at the observing time. Note that for the ADSSV results in Wu et al. (2009a) the observing time was equivalent to the model initial time (i.e., no forecast lead time is applied). Again, the issue of the TC location shift due to the perturbed initial condition is completely unrelated to the definition of response functions in the ADSSV since no other procedure would be conducted for the small change in the final-time TC location in the adjoint calculation.

b. Procedure of systematically perturbing the initial field

This paper focuses on how perturbations in the initial condition associated with the ADSSV sensitivity signals influence the simulated track and background steering flow. Identifying the appropriate way to perturb the model initial state remains an area of active research (Reynolds et al. 2008). Based on the perspective of ADSSV methodology, the procedure of systematically perturbing the initial field to maintain dynamical balance in the model initial condition (Wu et al. 2009d) is employed and briefly described in this subsection.

First, the relative vorticity at each individual level at the model initial time is increased (decreased) by a certain quantity (e.g., half of the original value in this paper) inside a certain perturbed domain. After the initial relative vorticity has been perturbed, the corresponding streamfunction is obtained with the modified relative vorticity by solving the equation $\nabla^2\psi = \varsigma$. Then, both zonal and meridional winds can also be acquired from the nondivergent flow component. Meanwhile, the new geopotential is obtained from the nonlinear balance equation and the temperature from the hydrostatic equation. Since the modified flow and mass fields are derived from the streamfunction related to the perturbed vorticity, they are the dynamically balanced state variables in the model initial condition for the perturbed experiments. Since the ADSSV represents the gradient of response functions (i.e., background steering flow) to the initial vorticity perturbation, this procedure is more directly connected to the ADSSV with respect to the vorticity field than other measures taken to perturb the initial field, such as SVs (Molteni et al. 1996) and ensemble transform (ET; Bishop and Toth 1999; McLay et al. 2007) techniques.

c. Experimental design

Following previous studies, this paper also examines the case of Typhoon Shanshan, initialized at 0000 UTC 15 September 2006. Two distinct ADSSV features associated with the midlatitude trough and the subtropical high (Fig. 1) that affect the recurving motion of Shanshan are identified. Based on the procedure to perturb the initial field as mentioned in section 2b, several experiments with perturbed and unperturbed [i.e., the control run (CTRL)] initial conditions are designed to examine how

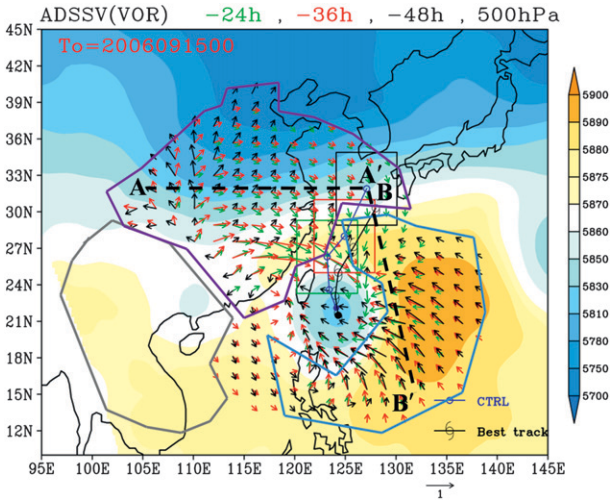

FIG. 1. ADSSV with respect to the vorticity field at 500 hPa at 24 (green), 36 (red), and 48 h (black) as verifying times, superposed with the geopotential height at 500 hPa at 0000 UTC 15 Sep 2006. The magnitude of ADSSV is normalized by the maximum value in the domain (values smaller than 0.25 are omitted). The three square boxes represent the verifying areas at corresponding verifying times. The best track and 48-h simulated track in CTRL are indicated by the black typhoon symbols and the blue circles for every 12 h, respectively. The perturbation regions associated with the midlatitude trough [DTR+ (−), STR+ (−)], the subtropical high [DSH+ (−), SSH+ (−)], and the low ADSSV sensitivity region [DNS+ (−)] are labeled by the purple, blue, and gray contours, respectively.

perturbations associated with high or low ADSSV signals would influence the model simulations and to physically interpret the significance of ADSSV sensitivity. Experiments with the perturbed initial conditions in the high sensitivity regions in which the normalized 24-, 36-, or 48-h ADSSV is larger than 0.25 associated with the midlatitude trough are denoted as DTR+ (−), while experiments associated with the subtropical high (see Fig. 1 regarding the initial vorticity perturbation region) are denoted as DSH+ (−). Note that the fields inside a domain with the 500-km radius centered at the TC are not perturbed in order for the TC structure and intensity to remain unchanged. Experiments with the low sensitivity smaller than 0.25 are also conducted and represented as DNS+ (−). For these experiments, the perturbed depth was chosen between 925 and 300 hPa (Table 1). The symbol "+ (−)" in the experiment title represents that the vorticity field within the perturbed domain is increased (decreased) by 50% of its original absolute value. In addition, major sensitive signals associated with the midlatitude trough occur in the mid-to-upper troposphere while the maximum ADSSV associated with subtropical high is located in the mid-to-lower troposphere, as shown in Fig. 5 in Wu et al. (2009a). Thus, experiments with perturbed depth between 600 and 300 hPa for the midlatitude trough and between 850 and 450 hPa for the subtropical high were conducted and denoted as STR+ (−) and SSH+ (−), respectively, to investigate the effect of perturbations specifically in the sensitive layer.

Moreover, in the field campaign such as T-PARC, an optimization time of 48 h is often utilized to calculate the targeted observation guidance for TCs. In addition, higher ADSSV sensitivity verified at 24 and/or 36 h mostly occurs closer to the storm than that verified at 48 h (see longer green and red vectors in Fig. 1). Therefore, a sensitivity test in which the threshold used to determine the perturbed area is designed as 0.6 based on the ADSSV verified at 48 h (black vectors in Fig. 1) is conducted to examine the effect of perturbations specifically located at the region of higher sensitivity values. As indicated by black vectors in Fig. 1, the region with the ADSSV sensitivity larger than 0.6 is mainly associated with the southwestern edge of the subtropical high, while it is quite limited at the trough region. Thus, the sensitivity test perturbed only for the area associated with the subtropical high is demonstrated and denoted as DSH+ (−)_0.6. Experiments conducted in this paper are summarized in Table 1.

The MM5 forward model is utilized for the 48-h TC simulation initialized at 0000 UTC 15 September 2006.

TABLE 1. Summary of the experiments simulated for a 48-h period initialized at 0000 UTC 15 Sep 2006. The symbol "+ (−)" in the experiment title indicates that the vorticity is increased (decreased) by 50% of its original absolute value.

Expt	Perturbed region	Perturbed depth
CTRL	Control run (no perturbation added in the initial condition)	
DTR+ (−)	Purple contour in Fig. 1 (associated with the midlatitude trough)	925–300 hPa
DSH+ (−)	Blue contour in Fig. 1 (associated with the subtropical high)	925–300 hPa
DSH+ (−)_0.6	Normalized ADSSV sensitivity at 48 h larger than 0.6 in Fig. 1 (associated with the subtropical high)	925–300 hPa
DNS+ (−)	Gray contour in Fig. 1 (associated with the low sensitivity area)	925–300 hPa
STR+ (−)	Same as DTR+ (−)	600–300 hPa
SSH+ (−)	Same as DSH+ (−)	850–450 hPa

The model configuration was set to correspond to the nonlinear model and the adjoint model in which the ADSSV was calculated for the purpose of performing consistent validation experiments. The domain has a resolution of 60 km, 85 × 115 (latitude by longitude) horizontal grid points, with 20 even-interval sigma levels in the vertical. The initial and boundary conditions are acquired from the National Centers for Environmental Prediction (NCEP) Global Forecast System (GFS) analysis, which has a horizontal resolution of 1° × 1°.

3. Results

a. ADSSV sensitivity and initial perturbation fields

Since the sensitivity of Shanshan's motion to the synoptic systems from the ADSSV perspective has been investigated, ADSSV sensitivity of the case conducted in this paper is briefly reviewed here. The ADSSV [throughout the paper, only the ADSSV with respect to vorticity field is shown, as in Eq. (1)] at 24 h (in green), 36 h (in red), and 48 h (in black) as the verifying times is shown in Fig. 1, superposed with the geopotential height at 500 hPa at the initial time. Those ADSSV signals represent the sensitive regions that would affect steering flows at 24, 36, and 48 h. Note that the ADSSV signals at different verifying times correspond well to one another and are collocated along with the midlatitude trough over north-central China and the subtropical high to the east of Shanshan. It is indicated that these two synoptic systems would likely have high impact on the steering flows beyond 24 h and thus lead to changes in track forecasts. As mentioned in section 2c, several experiments with perturbed initial conditions are conducted to evaluate the impact of those perturbations in regions with high or low ADSSV signals on model simulations.

Figure 2a shows the vorticity field and the geopotential height at 500 hPa in the control experiment (CTRL) at the initial time. The newly balanced geopotential height and wind vector difference relative to CTRL at 500 hPa in DTR+, DSH−, and DNS+ are shown in Figs. 2b, 2c, and 2d, respectively. In DTR+, the vorticity within the perturbed region in Fig. 1 associated with the midlatitude trough is increased by 50% with a maximum vorticity change of 500 hPa from 7.9×10^{-5} s^{-1} to 1.2×10^{-4} s^{-1}. The perturbation leads to the strengthening of the trough with denser and deeper geopotential contours (Fig. 2b) and a southward shift of its location. In addition, the large wind difference at 500 hPa occurs around the axis of the trough at about 35°N. In contrast, the perturbation in DTR− weakens the trough with flatter geopotential contours (figure not shown). The vorticity associated with the subtropical high in DSH− (blue contour in Fig. 1) is reduced by 50% with the maximum vorticity change at 500 hPa from -6.0×10^{-5} s^{-1} to -9.0×10^{-5} s^{-1}. The perturbation results in slight strengthening of the subtropical high (Fig. 2c) as compared to CTRL, and the large wind difference occurs to the south and southeast of the Shanshan's center. In contrast, the perturbation in DSH+ leads to the weakening of the subtropical high at its edge to the east of Shanshan (figure not shown). In addition to these two high ADSSV signals, the region with the low ADSSV signal (gray contour in Fig. 1) is also perturbed. For DNS+ in which the vorticity is increased by 50%, there seems to be a local low system located to the north of Hainan (Fig. 2d) while the perturbation in DNS− produces minor changes with respect to CTRL (figure not shown). The forward model is rerun with those newly perturbed initial conditions for 48-h simulation to explore the impact of perturbations with ADSSV signals.

b. Track simulations

This subsection examines how model-simulated tracks are impacted in the experiments with perturbed initial conditions. Figure 3a shows the 48-h tracks simulated by the forward model for experiments in which the perturbations are introduced to strengthen their original systems (i.e., DTR+, DSH−, DNS+, STR+, SSH−) and their track differences relative to CTRL at 24, 36, and 48 h as well as the 18–48-h mean differences are shown in Fig. 3b. The simulated TC center at 48 h in DTR+ is located farther northeast to that in CTRL, showing a higher translation speed than in CTRL after the recurvature, while the TC center in DSH− is shifted to the southeast of the TC center in CTRL. It is worth noting in Fig. 3a that the TC track in DTR+ after 6 h starts to deflect toward the east of the CTRL track, while the TC in DSH− continuously moves northward (or north northwestward), and then turns northeastward after 24 h. It indicates that the strengthened trough makes the TC turn northeast earlier, while the strengthened subtropical high to the east of the TC would likely lead to its farther northward motion. It is consistent with our physical intuition. In contrast, the TC centers in DNS+ remain approximately the same as CTRL throughout the 48-h simulation. From Fig. 3b, the track differences in DSH− relative to CTRL are about 122.3 and 94.1 km at 36 and 48 h, respectively, while it is larger than 700 km at 48 h in DTR+. However, the track difference of DNS+ is always smaller than 80 km in the simulation.

Figures 3c,d are the same as Figs. 3a,b, but for experiments in which the perturbations are introduced to weaken their original systems (i.e., DTR−, DSH+,

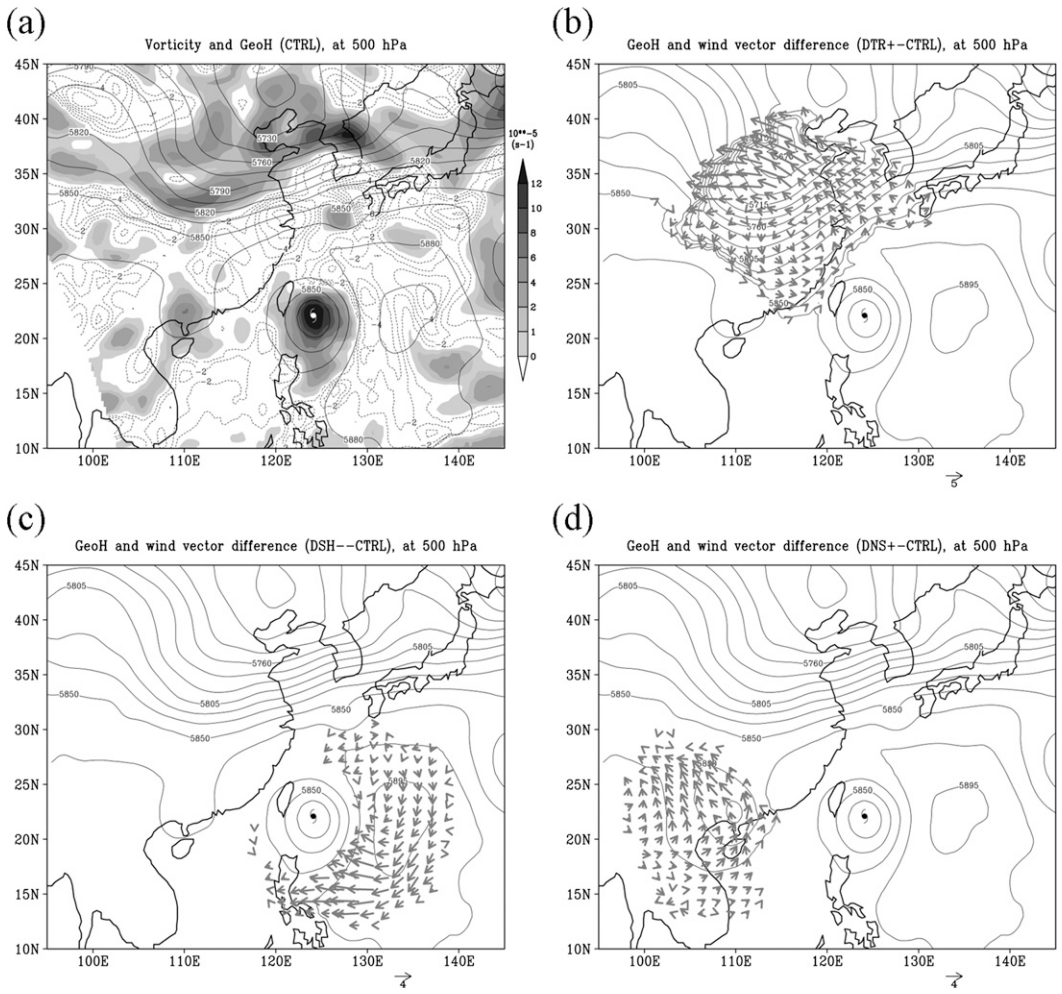

FIG. 2. At the model initial time (0000 UTC 15 Sep 2006): (a) the vorticity field (positive: shading; negative: dashed contour) and the geopotential height (solid contour with the 15-m interval) at 500 hPa in CTRL. The geopotential height (contour with the 15-m interval) and wind difference (vector; unit: m s^{-1}) relative to CTRL at 500 hPa: (b) DTR+, (c) DSH−, and (d) DNS+.

DNS−, STR−, SSH+). The simulated TCs in those experiments with weakened systems (Fig. 3c) appear to move more slowly as compared to those with strengthened systems (Fig. 3a). The TC in DTR− moves farther northward and then recurves northeastward after 36 h, with a track difference larger than 350 km at 36 h (Fig. 3d). It is indicated that the weakened trough would lead to late recurvature. Meanwhile, the simulated track in DSH+ exhibits eastward deflection after 24 h as well as slower movement as compared to CTRL. The TC center at 48 h in DSH+ is located to the south of that in CTRL with a track difference larger than 350 km (Fig. 3d). Similar to DNS+, the track in DNS− is not quite different from that in CTRL.

As mentioned in section 2c, the experiments STR+ (−) and SSH+ (−) are designed to examine the effect of perturbations specifically in the sensitive layer as compared to that in the deep layer. The impacts on the simulated tracks are also discussed here. It is shown that the TC at 48 h in STR+ is located to the northeast of that in CTRL, although it does not move northeastward as fast as the TC in DTR+ (Fig. 3a). Meanwhile, the TC in STR− appears to move more slowly than that in DTR−, showing a southward shift in the TC position at 48 h (Fig. 3c). In addition, the TC center at 48 h in SSH− is shown farther north as compared with DSH−, with the nearly 200-km track difference relative to CTRL (Figs. 3a,b). Note that in Figs. 3b,d, the 18–48-h mean track differences in STR+ (−) and SSH+ (−) are comparable with those in DTR+ (−) and DSH+ (−), respectively. It means that the synoptic system of the midlatitude trough (subtropical high) in which the

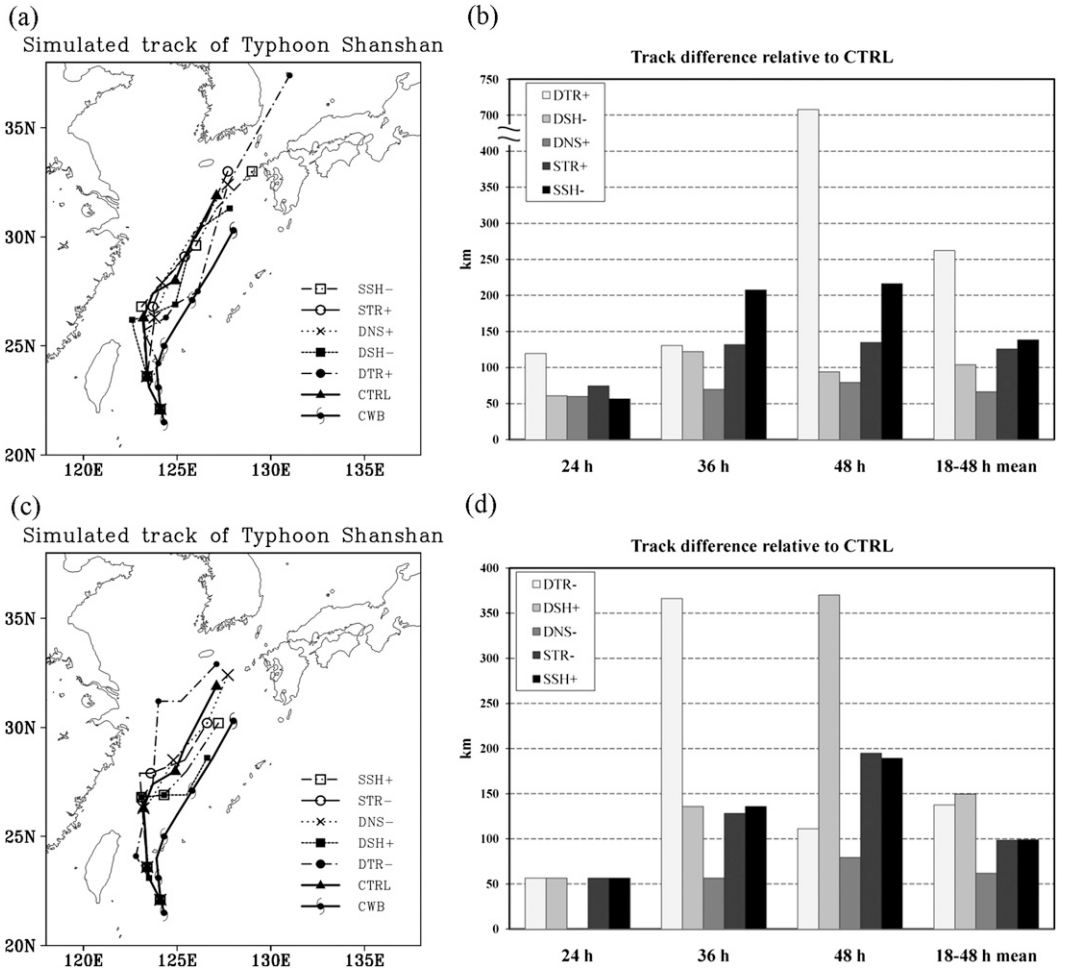

FIG. 3. (a) The best track (typhoon symbols) and the 48-h simulated tracks in CTRL (triangle), DTR+ (closed circle), DSH− (closed square), DNS+ (symbol "×"), STR+ (open circle), and SSH− (open square) for every 12 h. (b) The track difference relative to CTRL at 24, 36h, and 48 h as well as the 18–48-h mean difference in DTR+, DSH−, DNS+, STR+, and SSH−. (c),(d) As in (a),(b), but in DTR−, DSH+, DNS−, STR−, and SSH+.

perturbations are introduced in the mid-to-upper (mid-to-lower) troposphere based on the ADSSV signals has the same significance to the TC movement as the perturbations within the thicker depth (925–300 hPa). The effects of how the perturbations within the sensitive layer evolve will be discussed in section 3d.

The 18–48-h mean track differences (Figs. 3b,d) in DTR+ (−), DSH− (+), and DNS+ (−) relative to CTRL are 262.2 (137.5), 103.8 (149.4), and 66.6 (61.8) km, respectively. It is indicated that the perturbations associated with the trough and the subtropical high (deemed as high ADSSV sensitivity) lead to more track deflection than the perturbations in the region with low ADSSV sensitivity. This result is consistent with the ADSSV signals that measure sensitivity in the trough and the subtropical high and thereby determine the impacts on TC track simulation.

c. *Deep-layer-mean winds*

The well-known steering concept in Chan and Gray (1982) and numerous other publications in the literature state that TC motion is mainly controlled by the large-scale mean environmental flow across the TC. In addition, as indicated in the definition of the ADSSV, it represents the sensitivity of the mean background steering flow to the vorticity field at the initial time. Thus, how the steering flow of Shanshan is influenced by perturbations to the initial condition vorticity in various experiments is investigated in this subsection. To acquire large-scale environmental flows and remove the TC-scale circulation, the Lanczos filtering (Kim et al. 2009) is employed to calculate the 850–250-hPa DLM winds for different experiments. The similar way to perform the Lanczos filtering as in Kim et al. (2009) is adopted in this study. The total field can be

separated into a large-scale environmental field and a TC-scale field by the Lanczos filtering. By choosing the appropriate window length and cutoff frequency, components of the wavelength less than around 12°N are completely filtered out. The unrepresentative steering flow from the TC displacement effect as discussed in Hoover and Morgan (2010) does not exist here. Indeed, we have to reiterate that the result of the biased steering flow due to the TC location shift cannot be linked to the reliability of response functions defined in the ADSSV.

Figure 4 shows the evolution of the DLM wind difference relative to CTRL in DTR+ and DTR−. It can be seen that the DLM wind difference in DTR+ shows more eastward component around the TC after 24 h (Figs. 4b,c) and around the northward vector at 48 h (Fig. 4d). It is consistent with results shown by the simulated TC in DTR+, which moves to the northeast of CTRL, as discussed in section 3b. Moreover, the large track deflection in DTR+ (accelerating toward the northeast) would be likely related to the modification of wind field induced by the process of extratropical transition due to the strengthened midlatitude trough. In DTR−, the distinct anticyclonic flow pattern at the 12-h simulation time appears (Fig. 4e) due to the weakening of the trough. As time evolves, the southward or southwestward DLM wind difference around the TC after 36 h can be detected (Figs. 4g,h). It means that the weakened trough increases the southward component of the steering flow, slowing down the northward TC movement and leading to its late recurvature after 36 h. In both DTR+ and DTR− (Fig. 4), it can also be identified that the main feature of the DLM wind difference propagates along with the trough into the 48-h ADSSV verifying area (shown as the square box) throughout the 12–48-h simulation times. It can be noted that the initial vorticity perturbation associated with the trough in northern China would influence the DLM steering flow around Shanshan after 24 h. It is consistent with the ADSSV signals over the trough region in Fig. 1, indicating that the perturbation to the trough would affect the steering flow through 24–48 h. Furthermore, it is interesting to see that the impacts extend to the east of 130°E and farther downstream (top-right features in Figs. 4c,d,g,h).

The evolution of DLM wind difference between CTRL and DSH+ (−) is shown in Fig. 5. It shows that the main feature of wind difference in DSH+ is very limited at the beginning (Fig. 5a) and some signals with a westward component around the TC are shown at later stages (Figs. 5c,d), as compared to the results of DSH− (Figs. 5e–h). In contrast, the feature of wind difference in DSH− exhibits larger impacts around the TC as the strengthened high evolves with time. As a result of the strengthening of the high, a clear anticyclonic flow pattern to the east of TC appears at 12 h (Fig. 5e). The results at 12 and 24 h show that the northwestward component of DLM wind difference to the south of the TC continuously steer the TC (Figs. 5e,f), pushing the TC in DSH− farther northwest as compared with that in CTRL. At 48 h, the wind difference with the southeastward component in the verifying area is evident (Fig. 5h). Again, the feature of DLM wind difference in DSH− also evolves along with the TC and propagates into the verifying area following the model integration (Figs. 5e–h).

Figure 6 shows the evolution of DLM wind difference between CTRL and DNS+ (−). Comparing the results to those of DTR+ or DTR−, the DLM wind differences in DNS+ and DNS− are smaller. Although some signals appear within the verifying area in DNS+ (Fig. 6d), the DLM steering flow around the TC does not change significantly relative to CTRL before 36 h (Figs. 6a,b). As indicated in Fig. 2d, the perturbation in DNS+ produces local low around Hainan at the initial time. It is possible that the flow associated with DNS+ evolves and propagates downstream along with the midlatitude trough. In addition, this system might interact with the trough, modifying the flow from the trough. This is probably why impacts on the DLM wind at the final time can be detected around the TC in Fig. 6d. In DNS−, the DLM wind differences maintain a structure similar to the anticyclonic pattern from 12 to 36 h (Figs. 6e–g) and mainly stay to the west and southwest of the verifying area at 48 h (Fig. 6h). It indicates that the perturbation over the region with low ADSSV sensitivity has limited but nonnegligible effect on DLM steering flow during the 48-h simulation, leading to less track variation as discussed in section 3b. Nevertheless, it might have, to some degree, influence on the simulated TC beyond 48 h.

To examine and interpret the physical meaning of ADSSV, the study compares the ADSSV patterns and changes in the DLM steering flow around the TC at the verifying time because of the perturbations introduced in DTR+ (−), DSH+ (−), and DNS+ (−). The DLM steering change indicated by ADSSV associated with three perturbed regions and changes in the DLM steering flow relative to CTRL in various perturbed experiments are illustrated in Fig. 7. The ADSSV sensitivity is calculated by averaging the sensitivity values for 24 h (green vectors in Fig. 1), 36 h (red vectors in Fig. 1), and 48 h (black vectors in Fig. 1) as the verifying times over three perturbed regions indicated in Fig. 1 between 925 and 300 hPa. To maintain consistency with the magnitude of the DLM steering flow change, the steering change indicated by ADSSV is then derived from multiplying the average sensitivity value with the

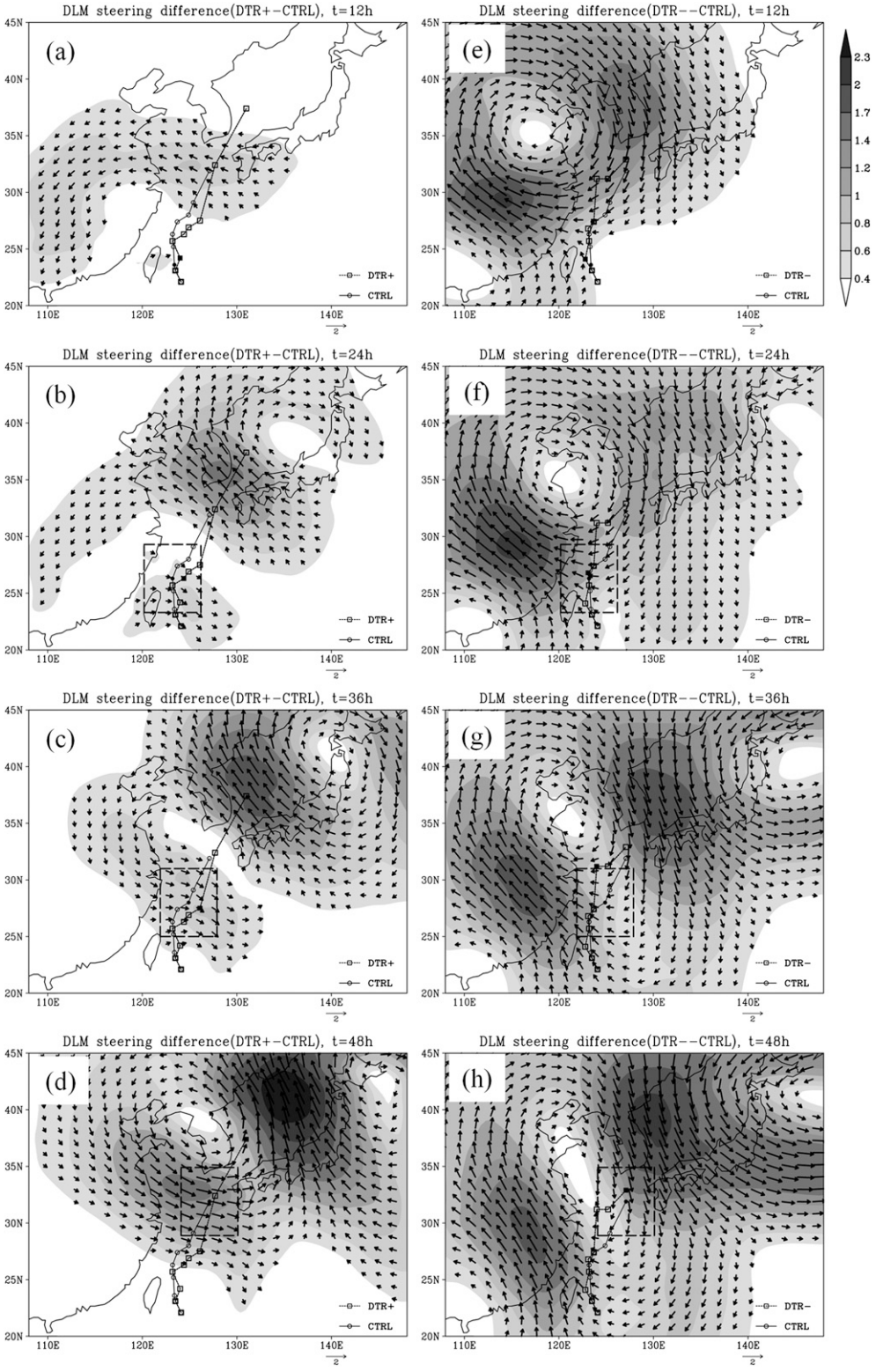

FIG. 4. The difference in the 850–250-hPa DLM steering flow (unit: m s^{-1}) relative to CTRL in DTR+ at (a) 12, (b) 24, (c) 36, and (d) 48 h, and in DTR− at (e) 12, (f) 24, (g) 36, and (h) 48 h. Wind with velocity above 0.4 m s^{-1} is shaded. The simulated tracks for perturbed experiments and CTRL are represented by open squares and open circles for every 6 h, respectively. The dashed square box represents the verifying area located at (b),(f) the 24-; (c),(g) 36-; and (d),(h) 48-h TC center in CTRL.

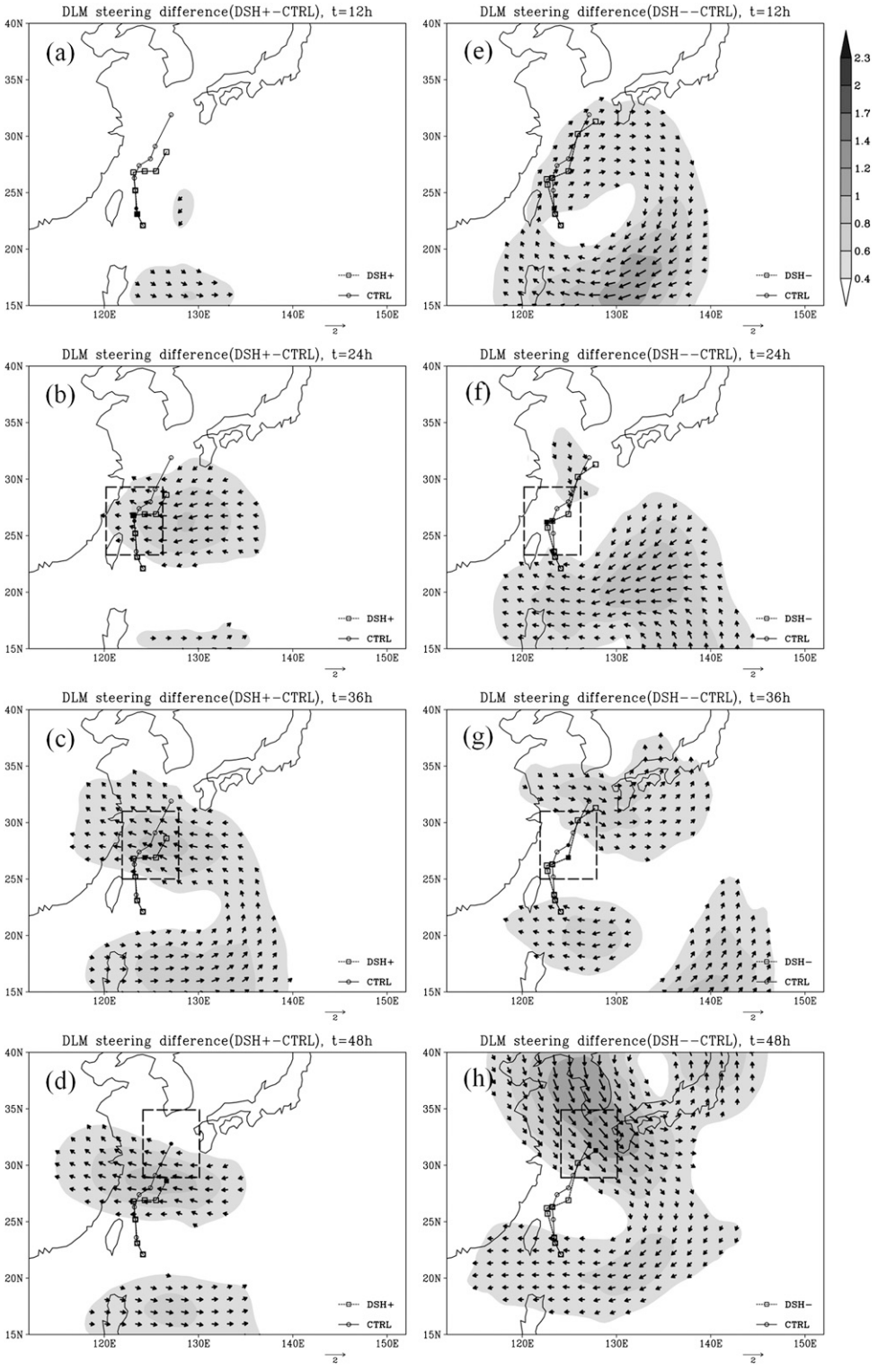

FIG. 5. As in Fig. 4, but in DSH+ at (a) 12, (b) 24, (c) 36, and (d) 48 h, and in DSH− at (e) 12, (f) 24, (g) 36, and (h) 48 h.

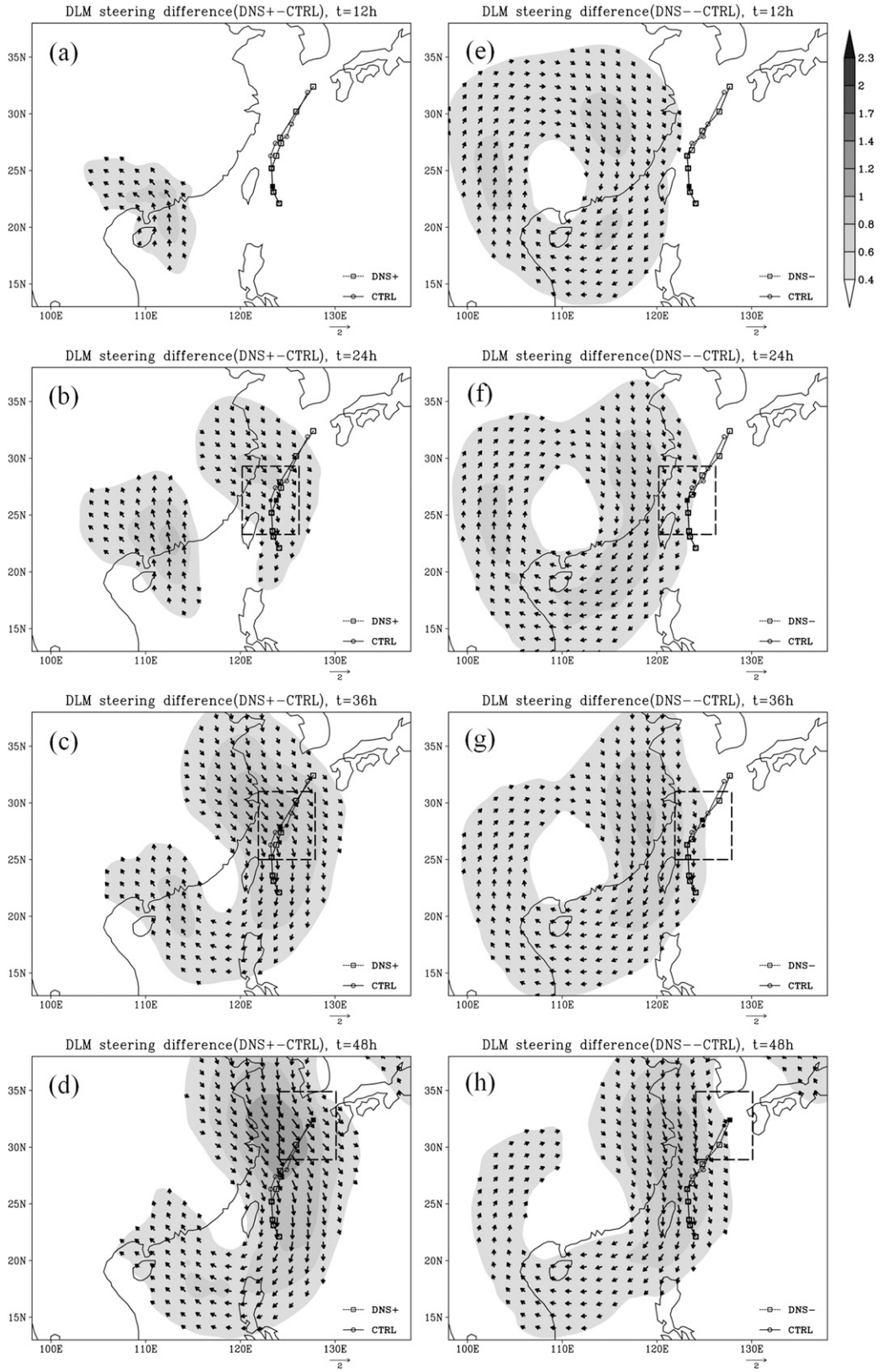

FIG. 6. As in Fig. 4, but in DNS+ at (a) 12, (b) 24, (c) 36, and (d) 48 h, and in DNS− at (e) 12, (f) 24, (g) 36, and (h) 48 h.

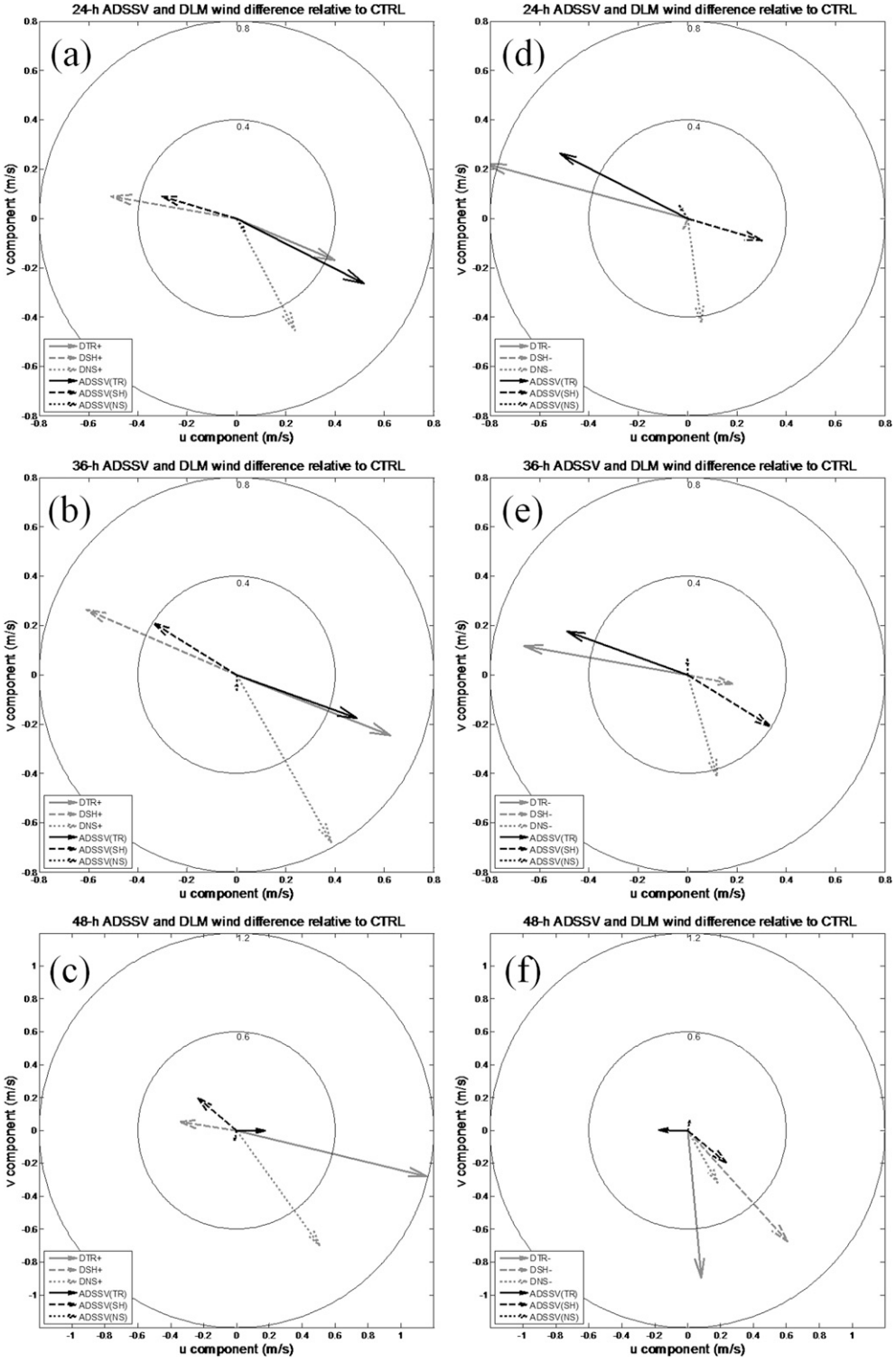

FIG. 7. The comparison between the difference of area-average DLM steering vector relative to CTRL within the verifying area in DTR+ (solid gray), DSH+ (dashed gray) as well as DNS+ (dotted gray) and the ADSSV w.r.t. vorticity increase averaged within three corresponding perturbation regions (solid, dashed, and dotted black) indicated in Fig. 1 at (a) 24, (b) 36, and (c) 48 h as the verifying times. (d),(e),(f) As in (a),(b),(c), but in DTR−, DSH−, as well as DNS− and the ADSSV w.r.t. vorticity decrease. The two circles represent the scales of 0.4 and 0.8 m s^{-1} in (a),(b),(d), and (e) [0.6 and 1.2 m s^{-1} in (c) and (f)].

mean vorticity change within three respective perturbed domains. Meanwhile, the areal average of the DLM steering flows in the perturbed experiments over the 24-, 36-, and 48-h verifying areas indicated by the green, red, and black squares in Fig. 1 is calculated after employing the Lanczos filtering. Consequently, both of them remain the same unit of wind speed (m s^{-1}).

The DLM steering change indicated by ADSSV with respect to vorticity increase (decrease) as well as the steering change due to increased (reduced) vorticity perturbations valid at 24, 36, and 48 h are shown in Figs. 7a,b,c (Figs. 7d,e,f), respectively. Focusing on the results associated with the perturbed region over the midlatitude trough, the comparison between the ADSSVs (solid black) and the DLM steering change vectors (solid gray) indicates that their directions are generally consistent with each other, but the bifurcation becomes large as time increases. For example, the direction of ADSSV with respect to vorticity decrease at 48 h as the verifying time (Fig. 7f) averaged over the perturbation region in northern China (associated with the trough) is pointing westward. Meanwhile, the DLM steering change in DTR− at 48 h (Fig. 7f) displays southward vector with southward bias. As for the perturbed region associated with the subtropical high, it is also shown that the DLM steering change (dashed gray) generally matches the corresponding direction of ADSSV (dashed black) relatively well, except for that in DSH− at 24 h (Fig. 7d) with the relatively small magnitude (less than 0.1 m s^{-1}). Meanwhile, the magnitude of DLM steering difference relative to CTRL ranges between 0.5 and 0.8 m s^{-1} in DNS+ and slightly smaller between 0.3 and 0.4 m s^{-1} in DNS− verified at 24, 36, and 48 h, which is relatively underestimated by the steering change derived from the ADSSV. The DLM steering change in DNS+ and DNS− through 24–48 h (dotted gray) is mostly pointing to the southeast or south, which is not well represented by the direction of ADSSV (dotted black). The reason why the simulated track in DNS+ (−) is almost the same as that in CTRL would be in part attributed to the cancellation between the southeastward steering flow difference and the northwestward drift induced by beta gyres. Regarding the relative contribution to changes in the DLM steering flows, the result in Fig. 7 indicates that the perturbations to the low ADSSV sensitivity region might have a nonnegligible impact. One speculation is that the initial perturbations are large so that the system may have strong interactions with the trough to the north and propagate downstream, as mentioned earlier. Such nonlinear process could not be accounted for and specified by the ADSSV, which is based on the assumption of linear calculation.

d. Vertical structure and evolution of kinetic energy

The effect of the evolvement of perturbations introduced specifically to the sensitive layer as compared with that in the whole deep layer is explored here. The vertical cross section of kinetic energy difference relative to CTRL along the line AA′ indicated in Fig. 1 in DTR+ and STR+ is shown in Fig. 8. It can be clearly identified that modifications of the trough mainly occur in the mid-to-upper troposphere, even when the perturbation is added only below 600 hPa in DTR+ at the initial time (Figs. 8a,e). As for our physical intuition, the feature of the midlatitude trough belongs to the system at high levels. At 12 h, the kinetic energy difference in STR+ expands toward 100 hPa and reaches a maximum of over 90 m^2 s^{-2} between 400 and 300 hPa (Fig. 8f). Meanwhile, it also propagates downward as quickly as that in DTR+ toward point A′ (Figs. 8b,f). After 24 h, the signal of kinetic energy difference in STR+ approaches the surface and shows a significant impact near point A′ below 500 hPa, similar to that in DTR+ (cf. Figs. 8c,d,g,h). It is indicated that the perturbation in the mid-to-upper troposphere associated with the trough grows and evolves along with the deep layer, leading to the comparable track change (Figs. 3a,b).

Figure 9 shows the vertical cross section of kinetic energy difference along the line BB′ indicated in Fig. 1 in DSH− and SSH−. It is observed that the large positive kinetic energy difference at high levels (above 450 hPa) is not included in SSH− at the initial time (Figs. 9a,e). It evolves and propagates toward point B, with a maximum positive kinetic energy difference around 600 hPa whereas the negative counterpart measures below 700 hPa at 12 h, which is similar to DSH− (Figs. 9b,f). At 48 h, the negative kinetic energy difference between 1000 and 600 hPa and the positive between 500 and 200 hPa around point B are shown in Fig. 9h. It is interesting that different from STR+, the development and propagation of perturbation in SSH− mainly concentrate in the mid-to-lower troposphere (Figs. 9g,h). Information associated with the subtropical high below the midlevel plays a significant role in producing track changes within the whole deep layer.

e. Sensitivity test—Impact from the area of higher ADSSV sensitivity

As mentioned in section 2c, the experiment of DSH+ (−)_0.6 where the normalized ADSSV verified at 48 h is larger than 0.6 associated with the subtropical high is conducted to explore the impact induced by perturbations in higher sensitivity area. The area in DSH+ (−)_0.6 is about one-third of that in DSH+ (−). The simulated track in DSH+ (−)_0.6 appears similar to that

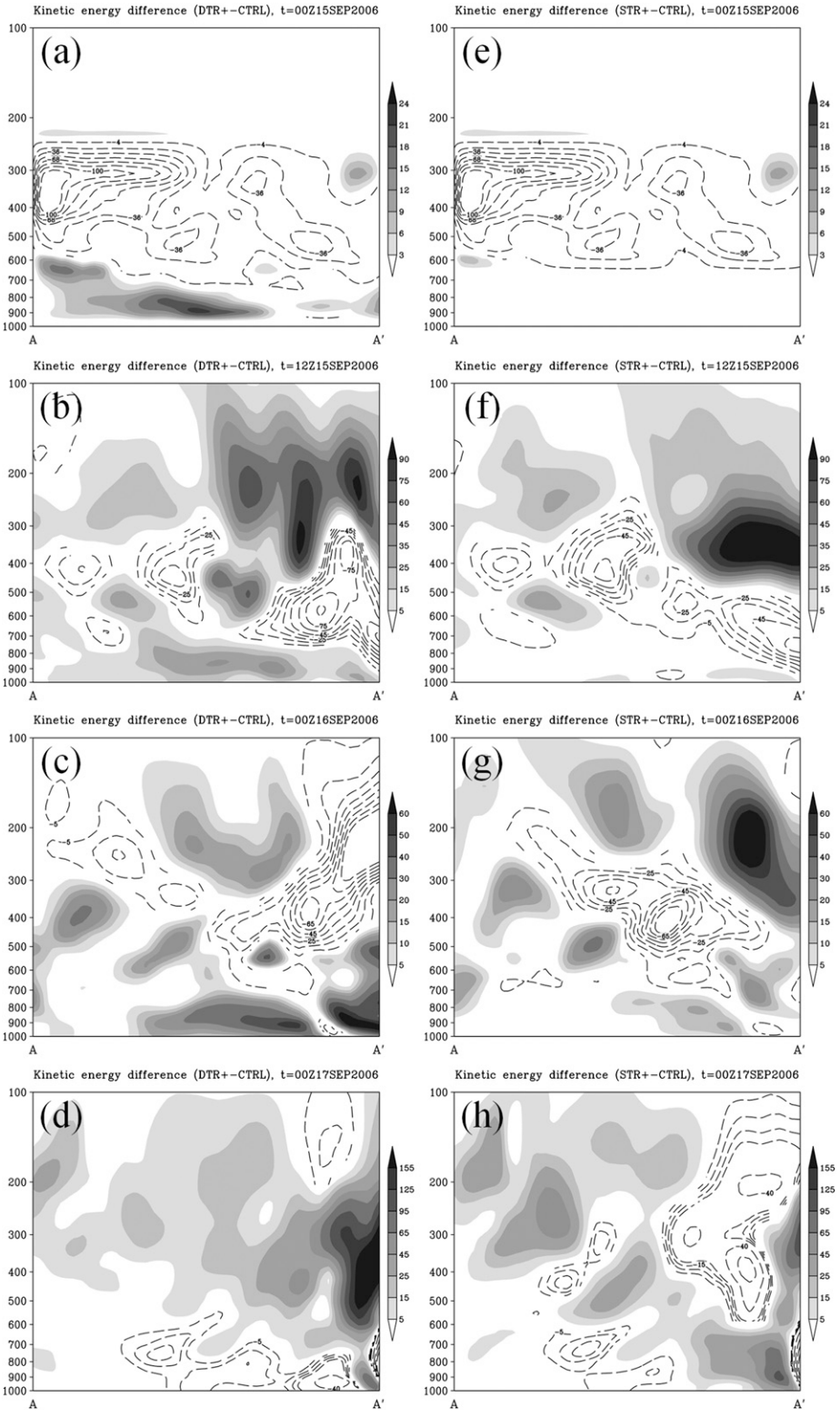

FIG. 8. Vertical cross sections of the kinetic energy difference relative to CTRL along the line AA′ indicated in Fig. 1 in DTR+ at (a) 0, (b) 12, (c) 24, and (d) 48 h, and in STR+ at (e) 0, (f) 12, (g) 24, and (h) 48 h. Shading (dashed contour) denotes positive (negative) values. The left and right ends of the abscissa in (a)–(h) correspond to A and A′ in Fig. 1, respectively. The ordinate (vertical pressure) is in logarithmic scale.

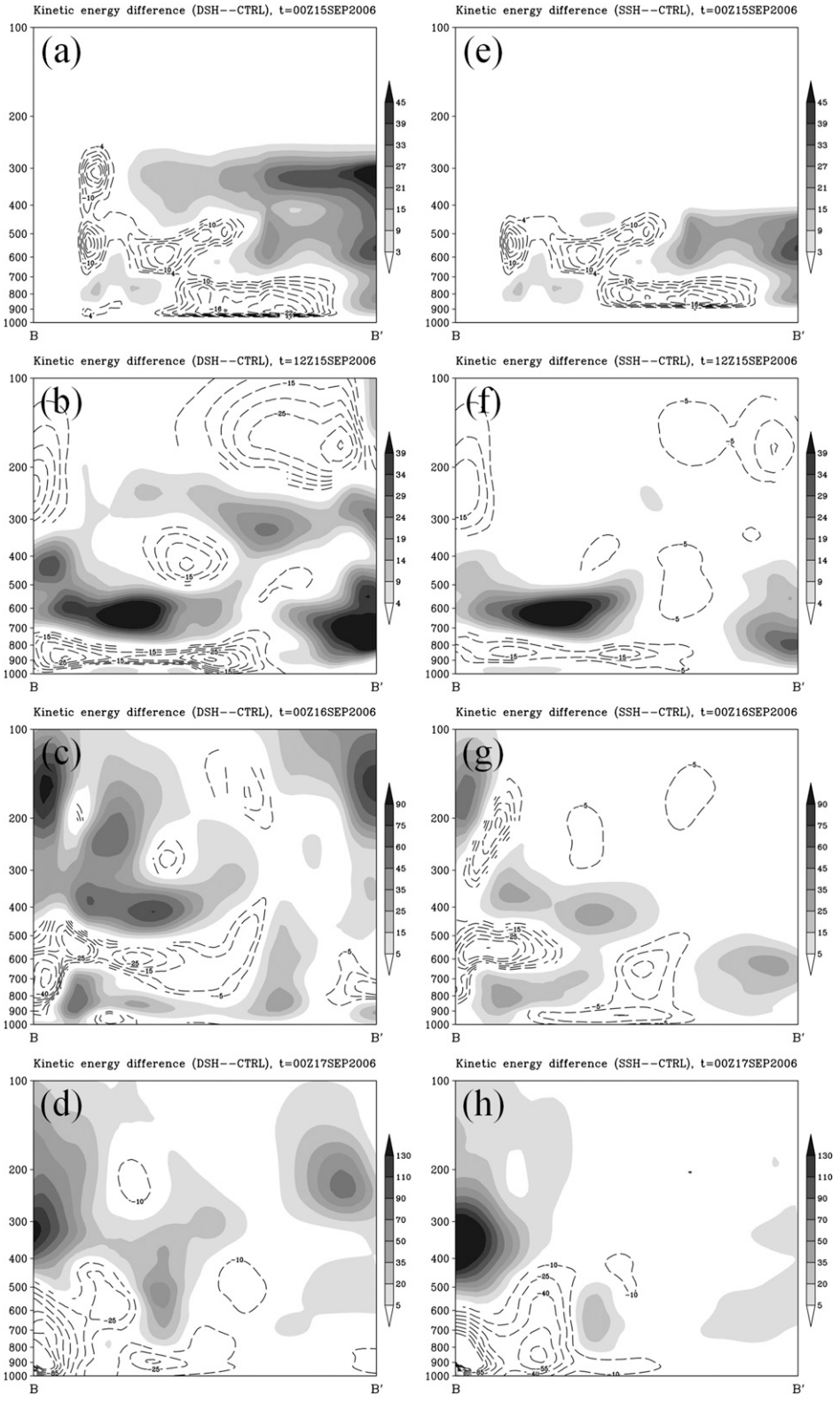

FIG. 9. As in Fig. 8, but in DSH− at (a) 0, (b) 12, (c) 24, and (d) 48 h, and in SSH− at (e) 0, (f) 12, (g) 24, and (h) 48 h along the line BB′ indicated in Fig. 1. The left and right ends of the abscissa in (a)–(h) correspond to B and B′ in Fig. 1, respectively.

in DSH+ (−). In addition, the track difference relative to CTRL in DSH+ (−)_0.6 is comparable and slightly larger than that in DSH+ (−) through 24–48 h (figure not shown). The 18–48-h mean track differences in DSH+ (−)_0.6 and DSH+ (−) are 160.7 (139.8) and 149.4 (103.8) km, respectively. It is indicated that the perturbation introduced within the smaller area of higher sensitivity values (larger than 0.6) leads to track deflection comparable to that in the larger area of the subtropical high.

Similar analysis as Fig. 5 is performed in DSH+ (−)_0.6. The signal of DLM wind difference in DSH+ (−)_0.6 can be identified within the verifying area at 48 h with the largest magnitude of about 0.7 (1.0) m s^{-1} (figure not shown). The areal-averaged magnitude of the DLM wind difference within the verifying area at 48 h in DSH+ (−)_0.6 is about 0.30 (0.56) m s^{-1}, which is generally comparable with that in DSH+ (−) of about 0.35 (0.91) m s^{-1}. It is indicated that the perturbation specifically located at the region of higher ADSSV sensitivity has similar and significant impacts on the DLM steering flows within the verifying area, as compared to that in the whole subtropical high system, thus leading to almost identical track changes. From the perspective of practical application of targeted observations, the results from this sensitivity test also suggest that because of the limited aircraft resources, the dropwindsonde observations taken only in high sensitivity area would likely provide better analysis fields, thus resulting in track forecast improvements.

4. Summary and discussion

As shown in Wu et al. (2009a), the ADSSV captures the synoptic features associated with the midlatitude trough and the subtropical high that affect the steering flow of Typhoon Shanshan (2006), leading to its recurvature. The influences from the two major features are also well validated by the PV diagnosis. In this study, the initial vorticity fields in regions with high or low ADSSV sensitivity are systematically perturbed at the initial time to investigate how those perturbations influence track simulation and the steering flow of Shanshan using the nonlinear MM5 forward model.

The results from the track simulation indicate that perturbations in regions with high ADSSV sensitivity cause more track deflection relative to the unperturbed control run (i.e., CTRL) than those with low ADSSV sensitivity. It is consistent with the ADSSV signals that pick up these two distinct synoptic features in terms of impacts on the TC track simulation. In addition, the perturbations introduced specifically to the sensitive layers lead to the comparable track changes as those in the deep-layer troposphere.

By performing the Lanczos filtering in different experiments, how perturbations to the initial vorticity influence the 850–250-hPa DLM wind is calculated and explored. With the Lanczos filtering employed, the mean environmental flows could be obtained and the TC-scale circulations are also removed. The unrepresentative steering flow from the TC displacement effect due to the perturbed initial condition, as discussed in Hoover and Morgan (2010), does not exist here at all.

It is shown that the signal of DLM wind difference relative to CTRL in experiments DTR+, DTR−, and DSH− evolves and propagates along with these perturbed synoptic systems into the 48-h ADSSV verifying area from 24 to 48 h. In DSH+, the limited wind difference pattern is found at the beginning and some impacts are shown at later stages. Although the signal of wind difference in DNS+ and DNS− exists in or around the verifying area, it appears to have larger impacts at later stages (after 42 h). Comparisons between the DLM steering change indicated by ADSSV associated with three perturbed regions indicated in Fig. 1 and changes in the DLM steering flow within the verifying area due to the initial vorticity perturbations are conducted at 24, 36, and 48 h as the verifying times. For the results associated with two perturbed regions with high ADSSV sensitivity, it is found that the change in the area-average DLM steering flow over the corresponding verifying areas generally has good agreement with the direction of ADSSV, except for DSH− valid at 24 h with a relatively small value. In addition, the degree of resemblance between the ADSSV and the DLM steering change appears increase with the shorter integration time. This is consistent with the concept that the ADSSV is calculated based on the linear assumption. Nevertheless, the DLM steering change for the perturbed region with low sensitivity is not well picked up by the ADSSV although it might have nonnegligible contributions. The nonlinearity of the process in which the large initial perturbations may interact with the trough to the north could not be well represented and signified by the ADSSV, which is calculated based on the linear assumption.

The vertical cross section of kinetic energy difference shows that the perturbation associated with the trough (subtropical high) introduced only between 600 and 300 hPa (850 and 450 hPa) evolves and develops similarly to the perturbation within the deep-layer troposphere (925–300 hPa), leading to the comparable track changes. This result well supports the vertical structure of ADSSV, demonstrating sensitivity to the trough (subtropical high) located in the mid-to-upper (mid-to-lower) troposphere [see Fig. 5 in Wu et al. (2009a)]. Furthermore, the sensitivity test in which the perturbed region is determined based on the normalized ADSSV sensitivity at

48 h larger than 0.6 is conducted. The results indicate that the perturbations specifically (locally) introduced in higher sensitivity area have the comparable effect on simulated track changes and the DLM steering flows within the verifying area, as compared to those in the broader area of the subtropical high. This sensitivity test provides useful insights on the validity of ADSSV as targeted observation guidance.

It should be noted that although this validation study is based on one single case, we believe this is still representative since two very distinct synoptic features are well captured by the ADSSV in this case. However, the statistical evaluation and validation of the ADSSV sensitivity requires more studies of characteristic cases with various dynamical systems affecting TC evolution. The procedure of perturbing the initial condition, such as using smaller vorticity perturbation based on the climatological variance of different systems, may also need to be examined. In addition, a targeted observation has been identified as one major issue in the field experiment, T-PARC, which has been successfully conducted from August to September in 2008 (Elsberry and Harr 2008). The unprecedented dataset would be valuable for further examination of the theory and the impact of targeted observations, as well as for improving understanding and forecasts of TCs.

Acknowledgments. The work is supported by the National Science Council of Taiwan through Grants NSC98-2111-M-002-008-MY3 and NSC97-2917-I-002-147, the Central Weather Bureau of Taiwan through Grant MOTC-CWB-98-6M-01, and the Office of Naval Research Grant N00173-08-1-G007. The authors thank Dr. Carolyn A. Reynolds of the Naval Research Laboratory for her helpful suggestions, as well as two anonymous reviewers for their constructive comments. The authors also thank Sun-Hee Kim and Joe Kwon of the Kongju National University in Korea for providing the Lanczos filtering program.

REFERENCES

Aberson, S. D., 2002: Two years of operational hurricane synoptic surveillance. *Wea. Forecasting,* **17,** 1101–1110.

——, 2003: Targeted observations to improve operational tropical cyclone track forecast guidance. *Mon. Wea. Rev.,* **131,** 1613–1628.

——, 2008: Large forecast degradations due to synoptic surveillance during the 2004 and 2005 hurricane seasons. *Mon. Wea. Rev.,* **136,** 3138–3150.

——, and J. L. Franklin, 1999: Impact on hurricane track and intensity forecasts of GPS dropwindsonde observations from the first-season flights of the NOAA Gulfstream-IV jet aircraft. *Bull. Amer. Meteor. Soc.,* **80,** 421–427.

Ancell, B., and G. J. Hakim, 2007: Comparing adjoint- and ensemble-sensitivity analysis with applications to observation targeting. *Mon. Wea. Rev.,* **135,** 4117–4134.

Bishop, C. H., and Z. Toth, 1999: Ensemble transformation and adaptive observations. *J. Atmos. Sci.,* **56,** 1748–1765.

——, B. J. Etherton, and S. J. Majumdar, 2001: Adaptive sampling with the ensemble transform Kalman filter. Part I: Theoretical aspects. *Mon. Wea. Rev.,* **129,** 420–436.

Buizza, R., and A. Montani, 1999: Targeted observations using singular vectors. *J. Atmos. Sci.,* **56,** 2965–2985.

Chan, J. C. L., and W. M. Gray, 1982: Tropical cyclone movement and surrounding flow relationships. *Mon. Wea. Rev.,* **110,** 1354–1374.

Chen, J.-H., M. S. Peng, C. A. Reynolds, and C.-C. Wu, 2009: Interpretation of tropical cyclone forecast sensitivity from the singular vector perspective. *J. Atmos. Sci.,* **66,** 3383–3400.

Elsberry, R. L., and P. A. Harr, 2008: Tropical cyclone structure (TCS08) field experiment science basis, observational platforms, and strategy. *Asia-Pac. J. Atmos. Sci.,* **44,** 209–231.

Errico, R. M., 1997: What is an adjoint model? *Bull. Amer. Meteor. Soc.,* **78,** 2577–2591.

Harnisch, F., and M. Weissmann, 2010: Sensitivity of typhoon forecasts to different subsets of targeted dropsonde observations. *Mon. Wea. Rev.,* **138,** 2664–2680.

Hoover, B. T., 2009: Comments on "Interaction of Typhoon Shanshan (2006) with the midlatitude trough from both adjoint-derived sensitivity steering vector and potential vorticity perspectives." *Mon. Wea. Rev.,* **137,** 4420–4424.

——, and M. C. Morgan, 2010: Validation of a tropical cyclone steering response function with a barotropic adjoint model. *J. Atmos. Sci.,* **67,** 1806–1816.

Kim, H. M., and B.-J. Jung, 2009a: Singular vector structure and evolution of a recurving tropical cyclone. *Mon. Wea. Rev.,* **137,** 505–524.

——, and ——, 2009b: Influence of moist physics and norms on singular vectors for a tropical cyclone. *Mon. Wea. Rev.,* **137,** 525–543.

Kim, S. H., H. J. Kwon, and R. L. Elsberry, 2009: Beta gyres in global analysis fields. *Adv. Atmos. Sci.,* **26,** 984–994.

Langland, R. H., 2005: Issues in targeted observing. *Quart. J. Roy. Meteor. Soc.,* **131,** 3409–3425.

Majumdar, S. J., C. H. Bishop, B. J. Etherton, and Z. Toth, 2002: Adaptive sampling with the ensemble transform Kalman filter. Part II: Field program implementation. *Mon. Wea. Rev.,* **130,** 1356–1369.

——, S. D. Aberson, C. H. Bishop, R. Buizza, M. S. Peng, and C. A. Reynolds, 2006: A comparison of adaptive observing guidance for Atlantic tropical cyclones. *Mon. Wea. Rev.,* **134,** 2354–2372.

——, S.-G. Chen, and C.-C. Wu, 2011: Characteristics of ensemble transform Kalman filter adaptive sampling guidance for tropical cyclones. *Quart. J. Roy. Meteor. Soc.,* **137,** 503–520.

McLay, J. G., C. H. Bishop, and C. A. Reynolds, 2007: The ensemble-transform scheme adapted for the generation of stochastic perturbations. *Quart. J. Roy. Meteor. Soc.,* **133,** 1257–1266.

Molteni, F., R. Buizza, T. N. Palmer, and T. Petroliagis, 1996: The ECMWF Ensemble Prediction System: Methodology and validation. *Quart. J. Roy. Meteor. Soc.,* **122,** 73–119.

Peng, M. S., and C. A. Reynolds, 2006: Sensitivity of tropical cyclone forecasts as revealed by singular vectors. *J. Atmos. Sci.,* **63,** 2508–2528.

Petersen, G. N., S. J. Majumdar, and A. J. Thorpe, 2007: The properties of sensitive area predictions based on the ensemble

transform Kalman filter (ETKF). *Quart. J. Roy. Meteor. Soc.,* **133,** 697–710.

Reynolds, C. A., M. S. Peng, S. J. Majumdar, S. D. Aberson, C. H. Bishop, and R. Buizza, 2007: Interpretation of adaptive observing guidance for Atlantic tropical cyclones. *Mon. Wea. Rev.,* **135,** 4006–4029.

——, J. Teixeira, and J. G. McLay, 2008: Impact of stochastic convection on the ensemble transform. *Mon. Wea. Rev.,* **136,** 4517–4526.

Weissmann, M., and Coauthors, 2011: The influence of assimilating dropsonde data on typhoon track and midlatitude forecasts. *Mon. Wea. Rev.,* **139,** 908–920.

Wu, C.-C., 2006: Targeted observation and data assimilation for tropical cyclone track prediction. *Proc. Sixth Int. Workshop on Tropical Cyclones,* San Jose, Costa Rica, WMO/CAS/WWW, 409–423.

——, and K. A. Emanuel, 1993: Interaction of a baroclinic vortex with background shear: Application to hurricane movement. *J. Atmos. Sci.,* **50,** 62–76.

——, T.-S. Huang, W.-P. Huang, and K.-H. Chou, 2003: A new look at the binary interaction: Potential vorticity diagnosis of the unusual southward movement of Typhoon Bopha (2000) and its interaction with Typhoon Saomai (2000). *Mon. Wea. Rev.,* **131,** 1289–1300.

——, and Coauthors, 2005: Dropwindsonde Observations for Typhoon Surveillance near the Taiwan Region (DOTSTAR): An overview. *Bull. Amer. Meteor. Soc.,* **86,** 787–790.

——, J.-H. Chen, P.-H. Lin, and K.-H. Chou, 2007a: Targeted observations of tropical cyclone movement based on the adjoint-derived sensitivity steering vector. *J. Atmos. Sci.,* **64,** 2611–2626.

——, K.-H. Chou, P.-H. Lin, S. D. Aberson, M. S. Peng, and T. Nakazawa, 2007b: The impact of dropwindsonde data on typhoon track forecasts in DOTSTAR. *Wea. Forecasting,* **22,** 1157–1176.

——, S.-G. Chen, J.-H. Chen, K.-H. Chou, and P.-H. Lin, 2009a: Interaction of Typhoon Shanshan (2006) with the midlatitude trough from both adjoint-derived sensitivity steering vector and potential vorticity perspectives. *Mon. Wea. Rev.,* **137,** 852–862.

——, and Coauthors, 2009b: Intercomparison of targeted observation guidance for tropical cyclones in the northwestern Pacific. *Mon. Wea. Rev.,* **137,** 2471–2492.

——, S.-G. Chen, J.-H. Chen, K.-H. Chou, and P.-H. Lin, 2009c: Reply. *Mon. Wea. Rev.,* **137,** 4425–4432.

——, K. K. W. Cheung, and Y.-Y. Lo, 2009d: Numerical study of the rainfall event due to interaction of Typhoon Babs (1998) and the northeasterly monsoon. *Mon. Wea. Rev.,* **137,** 2049–2064.

Yamaguchi, M., T. Iriguchi, T. Nakazawa, and C.-C. Wu, 2009: An observing system experiment for Typhoon Conson (2004) using a singular vector method and DOTSTAR data. *Mon. Wea. Rev.,* **137,** 2801–2816.

Zou, X., F. Vandenberghe, M. Pondeca, and Y.-H. Kuo, 1997: Introduction to adjoint techniques and the MM5 adjoint modeling system. NCAR Tech. Note NCAR/TN-435+STR, 110 pp. [Available from NCAR, P.O. Box 3000, Boulder, CO 80307-3000.]